Biomimetic coatings enhance tribocorrosion behavior and cell responses of commercially pure titanium surfaces

Isabella da Silva Vieira Marques[a)]
Department of Prosthodontics and Periodontology, Piracicaba Dental School, University of Campinas (UNICAMP), Av Limeira, 901, Piracicaba, São Paulo 13414-903, Brazil

Maria Fernanda Alfaro[b)]
Department of Restorative Dentistry, University of Illinois at Chicago, College of Dentistry, 801 S Paulina, Chicago, Illinois 60612

Miki Taketomi Saito[c)]
Department of Prosthodontics and Periodontology, Piracicaba Dental School, University of Campinas (UNICAMP), Av Limeira, 901, Piracicaba, São Paulo 13414-903, Brazil

Nilson Cristino da Cruz[d)]
Laboratory of Technological Plasmas, Engineering College, Univ Estadual Paulista (UNESP), Av Três de Março, 511, Sorocaba, São Paulo 18087-180, Brazil

Christos Takoudis[e)]
Departments of Chemical Engineering and Bioengineering, University of Illinois at Chicago, 851 S. Morgan St., SEO 218, Chicago, Illinois 60607

Richard Landers[f)]
Institute of Physics Gleb Wataghin, University of Campinas (UNICAMP), Cidade Universitária Zeferino Vaz, Barão Geraldo, Campinas, São Paulo 13083-859, Brazil

Marcelo Ferraz Mesquita[g)] and Francisco Humberto Nociti Junior[h)]
Department of Prosthodontics and Periodontology, Piracicaba Dental School, University of Campinas (UNICAMP), Av Limeira, 901, Piracicaba, São Paulo 13414-903, Brazil

Mathew T. Mathew[i)]
Department of Biomedical Sciences, University of Illinois, College of Medicine at Rockford, 1601 Parkview Avenue, Rockford, Illinois 61107

Cortino Sukotjo[j)]
Department of Restorative Dentistry, University of Illinois at Chicago, College of Dentistry, 801 S Paulina, Chicago, Illinois 60612

Valentim Adelino Ricardo Barão[k)]
Department of Prosthodontics and Periodontology, Piracicaba Dental School, University of Campinas (UNICAMP), Av Limeira, 901, Piracicaba, São Paulo 13414-903, Brazil

(Received 8 May 2016; accepted 28 July 2016; published 11 August 2016)

Biofunctionalized surfaces for implants are currently receiving much attention in the health care sector. Our aims were (1) to create bioactive Ti-coatings doped with Ca, P, Si, and Ag produced by microarc oxidation (MAO) to improve the surface properties of biomedical implants, (2) to investigate the TiO_2 layer stability under wear and corrosion, and (3) to evaluate human mesenchymal stem cells (hMSCs) responses cultured on the modified surfaces. Tribocorrosion and cell experiments were performed following the MAO treatment. Samples were divided as a function of different Ca/P concentrations and treatment duration. Higher Ca concentration produced larger porous and harder coatings compared to the untreated group ($p < 0.001$), due to the presence of rutile structure. Free potentials experiments showed lower drops (−0.6 V) and higher coating lifetime during sliding for higher Ca concentration, whereas lower concentrations presented similar drops (−0.8 V)

[a)]Electronic mail: isabellamarques@gmail.com
[b)]Electronic mail: mfalfaroc@gmail.com
[c)]Electronic mail: mikisaito@yahoo.com.br
[d)]Electronic mail: nilson@sorocaba.unesp.br
[e)]Electronic mail: takoudis@uic.edu
[f)]Electronic mail: landers@ifi.unicamp.br
[g)]Electronic mail: mesquita@unicamp.br
[h)]Electronic mail: nociti@fop.unicamp.br
[i)]Electronic mail: mtmathew@uic.edu
[j)]Electronic mail: csukotjo@uic.edu
[k)]Author to whom correspondence should be addressed; electronic mail: vbarao@unicamp.br

compared to an untreated group wherein the drop occurred immediately after the sliding started. MAO-treated surfaces improved the matrix formation and osteogenic gene expression levels of hMSCs. Higher Ca/P ratios and the addition of Ag nanoparticles into the oxide layer presented better surface properties, tribocorrosive behavior, and cell responses. MAO is a promising technique to enhance the biological, chemical, and mechanical properties of dental implant surfaces. © *2016 American Vacuum Society*. [http://dx.doi.org/10.1116/1.4960654]

I. INTRODUCTION

The use of dental implants in the rehabilitation of partially or totally edentulous individuals has increased in recent years as an alternative to conventional dental treatments.[1,2] Titanium (Ti) and its alloys are commonly used for dental implant applications due to their excellent biocompatibility and corrosion resistance. The thin oxide layer/passive film (TiO_2) generated when Ti is exposed to air inhibits corrosion processes and provides a superior interaction/interface with the surrounding tissues, preventing inflammatory responses.[3,4] However, this passive film may exhibit poor wear resistance.[5]

During mastication in an oral environment, dental implants are exposed to mechanical (i.e., wear), chemical (i.e., corrosion), and adverse biological effects, leading to a complex process of degradation.[6,7] In this way, a tribocorrosion phenomenon is characterized by the synergistic interaction of wear and corrosion, which may lead to implant failure and adverse biological reactions due to the release of wear debris and/or corrosion into the body.[8,9]

Some surface engineering techniques have been developed to create an enriched thick layer that can improve the surface characteristics, the tribological–corrosion properties, and biological responses.[3,10] Microarc oxidation (MAO) is considered a promising surface treatment to create rough, porous, and thick titania coatings, including strong bonding to the Ti substrate.[11]

Furthermore, this technique can incorporate different elements from the electrolytes into the oxide layer. Such elements can be calcium (Ca), phosphorous (P), silicon (Si), and silver (Ag), which may improve the biological response by promoting increased bone–implant contact, providing better healing and osseointegration,[10,12–14] and performing an antibacterial function.[10]

The oxide layer characteristics on the Ti surface can be modified by changing the parameters, such as voltage, frequency, duration, and the composition of the electrolytes.[16–19] However, further research is needed to characterize the oxide layers formed under different parameters such as the mechanical, chemical, and biological features so that one can identify the ideal conditions for the MAO process for dental applications.

The aims of this study were (1) to fabricate a bioactive Ti coating doped with Ca, P, Si, and Ag produced by MAO; (2) to investigate the TiO_2 layer stability under wear and corrosion during tribocorrosion experiments; and (3) to evaluate the cellular responses of human mesenchymal stem cells (hMSCs) cultured on the modified surfaces.

II. EXPERIMENT

A. Sample preparation

Commercially pure titanium (cpTi) disks (15 × 2 mm) were ground with 240–800 grit sandpaper (Carbimet 2, Buehler, Lake Bluff, IL, USA) and then a microfiber cloth (TextMet Polishing Cloth, Buehler) with diamond paste (MetaDi 9-micron, Buehler) and lubricant (MetaDi Fluid, Buehler) was used. Finally, colloidal silica suspension (MasterMet, Buehler) on polishing cloth (Chemomet I, Buehler) was used to achieve mirror finishing. The samples were degreased in an ultrasonic bath with 70% isopropanol and distilled water for 10 min. Two control groups were considered. A smooth surface was used as one control (untreated); the second consists of a sandblasted, large-grit, acid-etched (SLA) surface (Al oxide)[20,21] as a well-established surface treatment.

B. MAO coating preparation

MAO treatment was carried out using a pulsed DC power supply (Plasma Technology, Ltd., Kowloon, HK, China) for 5 and 10 min. The voltage, frequency, and duty cycle were set at 290 V, 250 Hz, and 60%, respectively. The aqueous mixtures were prepared using calcium acetate [$Ca(C_2H_3O_2)_2$], glycerophosphate disodium ($C_3H_7Na_2O_6P$) (Sigma-Aldrich, St. Louis, MO, USA), sodium silicate (Na_2SiO_3) (Vetec Quimica Fina Ltda, Duque de Caxias, RJ, Brazil), and Ag nanoparticles (<100 nm) (AgN; Sigma-Aldrich, St. Louis, MO, USA) (Table I). A total of eight experimental groups after MAO treatment was considered. After the MAO process, the samples were rinsed with deionized water and dried in warm air.

C. Surface characterization (morphology, chemical composition, and topography)

Three-dimensional images of 50 × 50 μm area were obtained to observe the topographies and profiles of all surfaces using an atomic force microscope (AFM, 5500 AFM/SPM, Agilent Technologies). A noncontact mode and two distinct areas of the samples were chosen for analysis. GWYDDION software was used for image processing. An x-ray diffractometer (XRD) (Panalytical, X'Pert Powder) using Cu-Kα ($\lambda = 1.540598$ Å), 45 kV, and 40 mA was used to determine the phase composition of the films. A microindentation test (HMV-2 Micro Hardness Tester, Shimadzu Corporation) was used to determine the Vickers microhardness of the cpTi disks. The Vickers microhardness values were obtained according to a previous report.[22] The Vickers hardness units (VHN) were calculated according to the following formula: VHN $2P = \sin(136°/2)/d2$, where P = load and d = diagonal length of indentations. The test was repeated four times in four randomly selected points on the surface. An average of these values represented the final Vickers microhardness value.

D. Tribocorrosion test protocol

After the surface treatment, the disks (n = 3/group) were placed in a custom-made electrochemical cell. Artificial

TABLE I. Experimental details of the treatments.

	Experimental groups							
	1-MAO				2-MAO			
	1-CaP5	1-CaP10	1-CaPAg5	1-CaPAg10	2-CaP5	2-CaP10	2-CaPSi5	2-CaPSi10
$Ca(CH_3CO_2)_2$	0.3 M	0.3 M	0.3 M	0.3 M	0.1 M	0.1 M	0.1 M	0.1 M
$C_3H_7Na_2O_6P$	0.02 M	0.02 M	0.02 M	0.02 M	0.03 M	0.03 M	0.03 M	0.03 M
Na_2SiO_3							0.04 M	0.04 M
Ag			0.62 g/l	0.62 g/l				
Treatment duration (min)	5	10	5	10	5	10	5	10

saliva with normal *p*H (6.5) was used as an electrolyte to simulate oral environmental conditions. The chemical composition for the artificial saliva was KCl (0.4 g/l), NaCl (0.4 g/l), $CaCl_2{\cdot}2H_20$ (0.906 g/l), $NaH_2PO_4{\cdot}2H_2O$ (0.690 g/l), $Na_2S{\cdot}9H_2O$ (0.005 g/l), and urea (1.0 g/l), based on previous studies.[24,25] A tribometer (DUCOM-Material Characterization Systems, Evanston, IL, USA) coupled with a potentiostat (SP-240 Bio-Logic, LLC, Knoxville, TN, USA) was used to conduct tribocorrosion experiments, which were performed using the standard three-electrode corrosion cell system.[26] A saturated calomel electrode was used as the reference electrode, a graphite rod as the counter electrode, and the exposed area of the sample as a working electrode. A ball-on-disk tribosystem with a 3/8 in. Al_2O_3 ball was used. The number of cycles (2000 cycles), frequency (1 Hz), and temperature (37 °C) parameters were selected to simulate the oral environments under 8.5 N load and 3 mm stroke [Hertzian contact pressure estimation of 800 MPa; Fig. 1(a)].

Our tribocorrosion tests were performed in two different modes: (1) free potential mode (when no potential is applied, and the changes in potential are monitored as a function of sliding period) and (2) potentiodynamic mode. Free potential mode gives information about the electrochemical state of the surface, but limited information on the kinetics of its reactions.[27] The test sequence was mainly divided into three stages: (1) initial stabilization period; (2) sliding period; and (3) final stabilization period, as described in Fig. 1(b). During the potentiodynamic experiments, the samples were polarized from −0.8 to 1.8 V at a scan rate of 5 mV s^{-1}. The initial stabilization started with a cleaning phase at a constant voltage of −0.9 V for 300 s. Afterward, the coefficient of friction (COF) and potential were monitored during the sliding period.

The film morphologies after sliding of inside and outside of the wear scar were observed with scanning electron microscopy (SEM: JEOL, JSM-6010LA), and the chemical composition was evaluated with an energy dispersive x-ray spectroscopy device attached to the SEM.

A white light interferometry (WLI) microscope was used to analyze the wear scar and to quantify the total mass loss after tribocorrosion experiments based on the wear scar

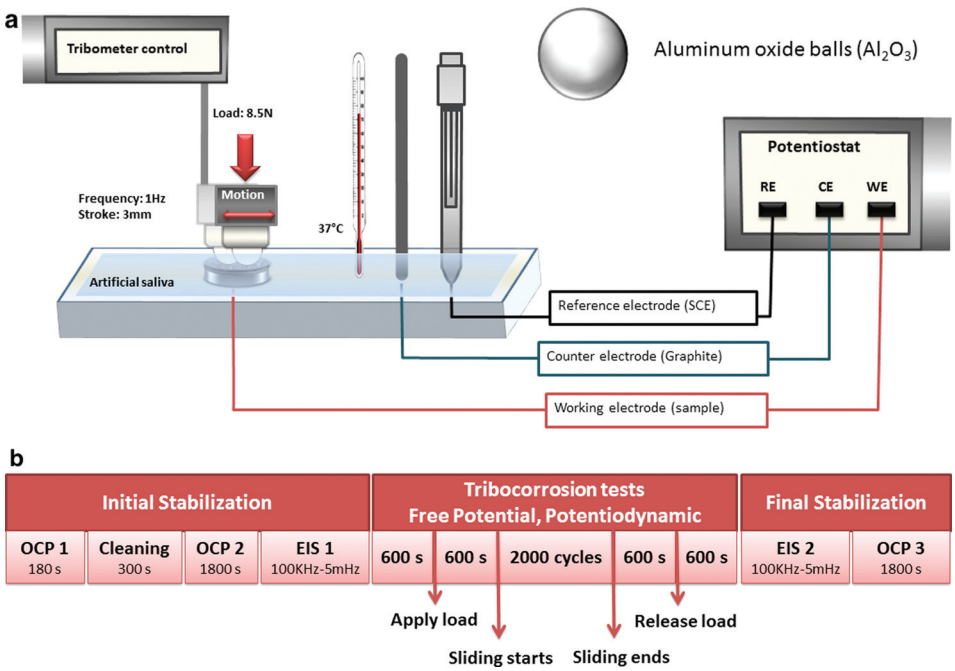

FIG. 1. (a) Schematic illustration of the tribocorrosion setup. (b) Tribocorrosion protocol during free potential and potentiodynamic experiments.

depth and volume. In addition, the surface roughnesses (Ra) of the inside and outside area of the wear scar were determined (Zygo New View 6300, Zygo Corporation).

E. Biological tests

1. Cell culture

hMSCs derived from adult bone marrow were provided by Tulane University. HMSCs were cultured in 100 mm culture dishes using Dulbecco's modified Eagle medium (DMEM: Gibco, Life Technologies) supplemented with 10% fetal bovine serum (FBS) (Gibco, Life Technologies), penicillin (100 U/ml), and streptomycin (100 mg/ml: Gibco, Life Technologies; DMEM + 10% FBS) in a humidified incubator at 37 °C and 5% CO_2 atmosphere. After reaching confluence (70%–80%), the cells were detached using trypsin-ethylenediaminetetraacetic acid (Gibco, Life Technologies), centrifuged, and resuspended in culture medium for seeding over the sterilized materials. Cells from the third to fifth passages were used in the experiments. For the cell culture experiments, new disks with four selected coating groups (untreated, Al oxide, 1-CaP10, 1-CaPAg10) were sterilized in ethylene oxide gas and used each time.

2. SEM analysis

To evaluate the morphology of hMSCs cultured on the titanium disks, a scanning electron microscope (JEOL, JSM5600LV, Japan) was used. Briefly, the disks were placed into 24-well plate (Corning Costar, USA), and hMSCs were seeded (2×10^4 cells/ml) over the disks with DMEM + 10% FBS and incubated in a humidified incubator at 37 °C and 5% CO_2 for 24 h to allow cell adhesion on the disks. After this period, the medium was replaced with fresh DMEM + 10% FBS, and the specimens were evaluated on days two and four. For the SEM analysis, the samples were fixed with Karnovsky's solution (*p*H 7.4) overnight at 4 °C and postfixed in 1% osmium tetraoxide in distilled water for 1 h at room temperature. Then, they were dehydrated through a graded ethanol series (35%, 50%, 70%, 90%, and 100%) at room temperature for 10 min each. Finally, the samples were critical-point dried (Denton Vacuum, mod. DCP-1, Moorestown, NJ, USA) and gold sputtered (Bal-Tec, mod. SCD 050, Fürstentum, Liechtenstein).

3. Fluorescence analysis

Cells attachment, spreading, and morphology were observed under fluorescence microscope (Leica DMI6000 B, Leica) after 3 h, 1 day, and 6 days. For fluorescent imaging, hMSCs were seeded at a density of 1.3×10^5 cells/ml. After washing the samples in phosphate buffer saline (PBS), the cells were fixed with 3.7% formaldehyde for 20 min, and permeabilized in 0.05% Triton X100 in PBS for 15 min. The cell cytoskeleton was stained with ActinRed™ 555 ReadyProbes® Reagent (Molecular Probes, Life Technologies) for 30 min, and the nucleus was stained with NucBlue® Fixed Cell ReadyProbes® Reagent (Molecular Probes, Life Technologies) for 20 min. The samples were washed in PBS twice again before the microscopic observations.

4. MTT assay

For metabolic analysis, hMSCs were seeded (3×10^4 cells/ml) over coated disks in a 24-well plate (Corning Costar, USA) using DMEM + 10% FBS, and incubated in a humidified incubator at 37 °C and 5% CO_2 for 24 h, to allow cell adhesion to the disks. After this period, the medium was replaced with fresh DMEM + 10% FBS, and this time point was considered the time 0 h for the MTT assay. The metabolic activity of the cell on the experimental groups was evaluated at 1, 3, and 6 days. After the experimental period, the medium was removed and replaced by 900 μl of DMEM and 100 μl of MTT (5 mg/ml) (Life Technologies, USA) at 37 °C, and 5% CO_2 for 4 h, protected from light. Subsequently, 500 μl of dimethyl sulfoxide (Sigma-Aldrich, USA) was added to each well to dissolve the formazan crystals, which were produced by the cleavage of MTT salt in the mitochondria of viable cells. Three aliquots of 100 μl of each sample were transferred into a 96-well plate, and the absorbance was determined at 540 nm using an Elisa microplate reader (VersaMax, Molecular Devices, Sunnyvale, CA, USA). The mean of the three readings of each 96-well plate was considered as a single value of the 24-well plate.

5. Matrix formation analysis

Sirius Red/Fast Green Collagen Staining kit (Amsbio, UK) was used to assess the quality of the extracellular matrix formed by hMSCs cultured on the disks. The disks were placed into 24-well plates (Corning Costar, USA), and hMSCs were seeded (7×10^4 cells/ml) over the disks using DMEM + 10% FBS and maintained in a humidified incubator at 37 °C and 5% CO_2. The collagenous and noncollagenous contents of the extracellular matrix were assessed at days 10 and 17, following the manufacturer's instructions. Briefly, the samples were washed with Dulbecco's PBS (Gibco, USA), then fixed with Kahle fixative solution for 10 min at room temperature, and washed with PBS. Subsequently, the samples were completely immersed in 200 μl of dye solution/well for 30 min at room temperature. The dye solution was removed, the samples were washed five times with distilled water, and then 1 ml of extraction buffer/well was added to each well. Aliquots (100 μl) of the mixed buffer of each well were transferred to a 96-well plate, and the absorbance was determined at 540 and 605 nm using an Elisa microplate reader (VersaMax, Molecular Devices, Sunnyvale, CA, USA). The mean of the three readings of each 96-well plate was considered as a single value of the 24-well plate. The amount of collagenous and noncollagenous proteins was determined according to the manufacturer's instructions.

6. qRT-PCR analysis

Quantitative reverse transcription polymerase chain reaction (qRT-PCR) was used to determine the messenger ribonucleic acid expression levels of osteogenic genes for hMSCs cultured on the controlled and modified cpTi disks. The hMSCs were cultured for 14 days in a previous culture medium, enriched with 0.05 mM L-ascorbic acid, 100 nM dexamethasone, and 10 mM β-glycerophosphate disodium salt hydrate to allow osteoblastic cell differentiation. The RNeasy Plus Mini Kit (Qiagen, Qiagen Sciences) was used to extract the total ribonucleic acid (RNA). The RNA concentration was detected by a spectrophotometer (Nanodrop 1000, Thermo Scientific), and complementary deoxyribonucleic acid was generated using RT^2 First Strand Kit for reverse transcription polymerase chain reaction (RT-PCR) (Qiagen, Qiagen Sciences). Quantitative real-time PCR was performed with FastStart Universal SYBR Green Master (Roche, Roche Diagnostics GmbH) and human osteogenic primers (Table II) using an ABI StepOnePlus instrument. The expression levels of alkaline phosphatase (ALP), osteocalcin (OC), runt-related transcription factor 2 (RUNX-2), Collagen-1 (Col-1), bone morphogenetic protein 2 (BMP-2), transforming growth factor beta 1 (TGF-β1), and glyceraldehyde 3-phosphate dehydrogenase (GAPDH) were analyzed. GAPDH was used as an internal reference. The relative gene expression level was estimated by transforming the logarithmic values into absolute values using $2^{-\Delta\Delta CT}$, where the average threshold cycle (CT) values were used to quantify the gene expression in each sample: $\Delta CT = \Delta CT\ (\text{target}) - \Delta CT\ (\text{GAPDH})$.

F. Statistical analysis

Analysis of variance was used to analyze the significant difference between groups for all analyses. Tukey's honestly significant difference (HSD) test was used as well for a multiple-comparison technique when needed. Correlation analysis between Vicker's microhardness and total mass loss was examined using Pearson's correlation test. $P \leq 0.05$ was used for all tests (SPSS v. 20.0; SPSS Inc.).

III. RESULTS AND DISCUSSION

A. Surface characterization

Porous oxide layers enriched with bioactive elements were obtained. Our previous study[23] evaluated the chemical composition of the outermost oxide layer of surfaces by XPS. The analysis indicated the presence of Ti, O, Ca, P, Si, and Al in the survey spectra. Also, the formation of calcium phosphate compounds[32–34] was suggested. Figure 2 shows AFM surface topographies and profiles of the controls and MAO-treated samples. There are some abrasion grooves on the cpTi polished surface. In all treated groups, a porous surface can be observed due to the dielectric breakdown during the surface treatment.[3,28,29] Interestingly, different electrolytes produced different porous configurations on the surface.[30] Larger pore sizes with deeper valleys and thicker oxide layers were observed when higher calcium acetate concentration (1-MAO) was employed in the MAO mixture. The valley depth values ranged from 2.53 to 2.86 μm for 1-MAO groups, from 0.78 to 1.08 μm for 2-MAO groups, a value of 0.25 μm for the untreated group, and 2.11 μm for the Al oxide group. The incorporation of Ca into the oxide layers is proportional to the calcium acetate concentration in the electrolyte.[29,31] In 2-MAO groups, the pores are smaller than in the 1-MAO groups, which may influence other surface properties.

The phase composition of Ti surface corresponding to each group was analyzed with the XRD spectra. The XRD spectra of the samples can be observed in Fig. 3. All MAO-treated samples presented anatase phase, while peaks of rutile phase were detected only for higher calcium concentrations (1-MAO). The presence of rutile crystalline structure may provide superior wear resistance due to the good adhesion with the substrate and the increase in thickness. Rutile leads to the production of harder coatings.[5] Figure 4(a) shows the microhardness values and total mass loss of all groups. Pearson's

TABLE II. Quantitative PCR genes and primer sequences.

Genes	Accession number		Primer sequences (5′ to 3′)
ALP	NM_000478.4	Forward	ACTGGTACTCAGACAACGAGA
		Reverse	ACGTCAATGTCCCTGATGTTATG
BMP-2	NM_001200.2	Forward	ACTACCAGAAACGAGTGGGAA
		Reverse	GCATCTGTTCTCGGAAAACCT
OC	NM_000234.2	Forward	CACTCCTCGCCCTATTGGC
		Reverse	CCCTCCTGCTTGGACACAAAG
Col-1	NM_000088.3	Forward	GAGGGCCAAGACGAAGACATC
		Reverse	CAGATCACGTCATCGCACAAC
RUNX2	NM_001024630.3	Forward	TGGTTACTGTCATGGCGGGTA
		Reverse	TCTCAGATCGTTGAACCTTGCTA
TGF-β1	NM_000660.5	Forward	CAATTCCTGGCGATACCTCAG
		Reverse	GCACAACTCCGGTGACATCAA
GAPDH	NM_002046.5	Forward	ACAACTTTGGTATCGTGGAAGG
		Reverse	GCCATCACGCCACAGTTTC

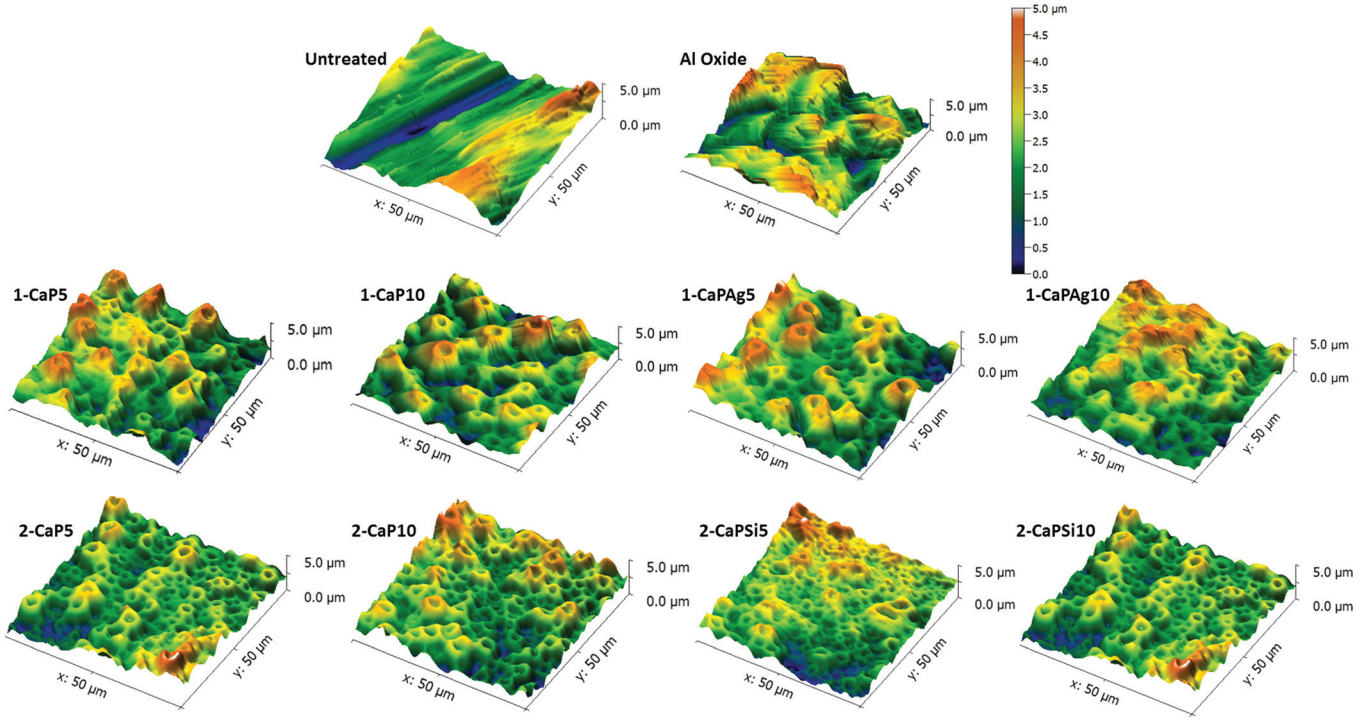

FIG. 2. Three-dimensional images of atomic force microscopy of cpTi disks after different surface treatments: Controls (untreated; Al oxide); 1-MAO (1-CaP5; 1-CaP10; 1-CaPAg5; and 1-CaPAg10); and 2-MAO (2-CaP5; 2-CaP10; 2-CaPSi5; and 2-CaPSi10).

correlation test revealed an inverse relationship between them [$r = -0.9705$, $p < 0.001$; Fig. 4(b)]. The hardest surface with the lowest mass loss was observed in the Al oxide group, followed by 1-MAO treated samples. Regarding MAO surface treatment, harder coatings were obtained in the presence of higher Ca concentrations. Significant differences were attained compared to the control group ($p < 0.05$).

B. Tribocorrosion tests

The evolution of open circuit potential (OCP) is shown in Fig. 5. Different values of OCP can be observed before sliding time (2000 s) between untreated and all treated groups, which demonstrates the improvement of corrosion tendency after surface treatment. The untreated group showed values around −0.4 V, whereas the treated groups

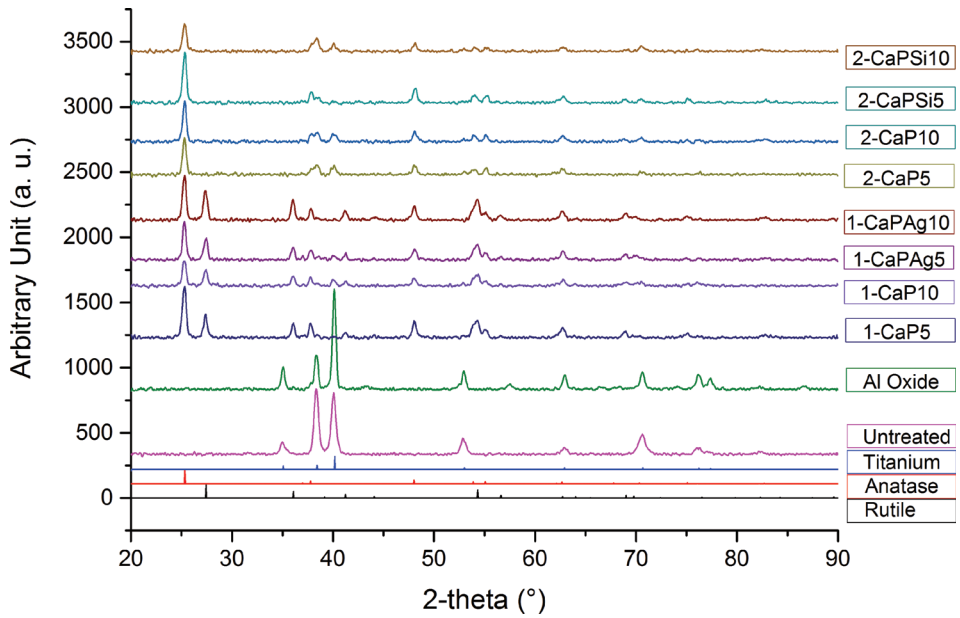

FIG. 3. X-ray diffraction patterns of cpTi for control (untreated) and MAO-treated samples. XRD baselines for titanium (PDF#00-044-1294), anatase TiO_2 (PDF#01-071-1166) and rutile TiO_2 (PDF#00-021-1276) are also provided.

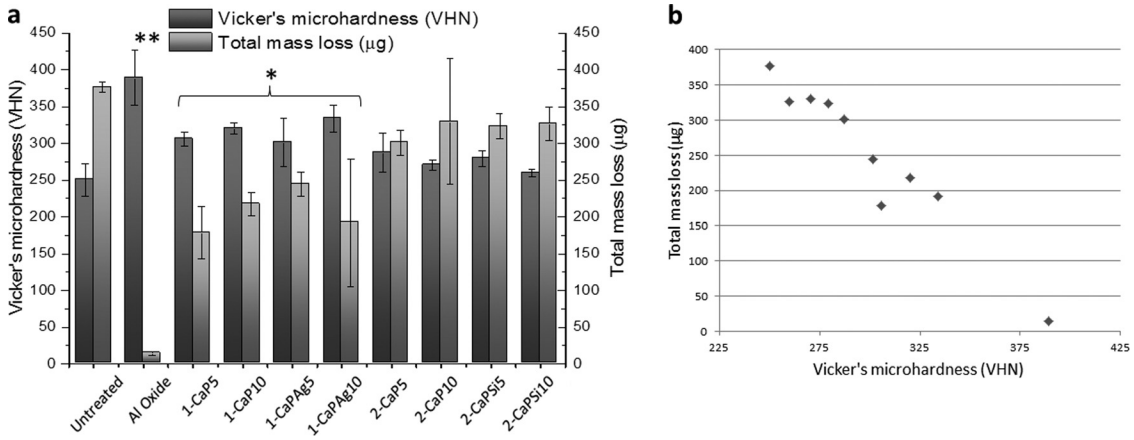

FIG. 4. (a) Vickers microhardness (VHN) and total mass loss (μg) after tribocorrosion experiments mean values; (b) correlation between them of all studied groups. A significant difference was noted with the untreated group (*$p < 0.05$; **$p \leq 0.001$; Tukey HSD test).

exhibited greater values (≈ -0.05 V). It is known that higher OCP values are related to noble characteristics of materials.[8,28] Hence, it is evident that MAO surface treatment was able to enhance the corrosion tendency of the Ti surface. Important differences were also encountered during the sliding period within the studied groups. Potential values tended to drop sharply when the specimen's surface faced mechanical stress, indicating the onset of wear. Once the stress stopped, there is a potential recovery (V rec) toward more anodic values.[35–40]

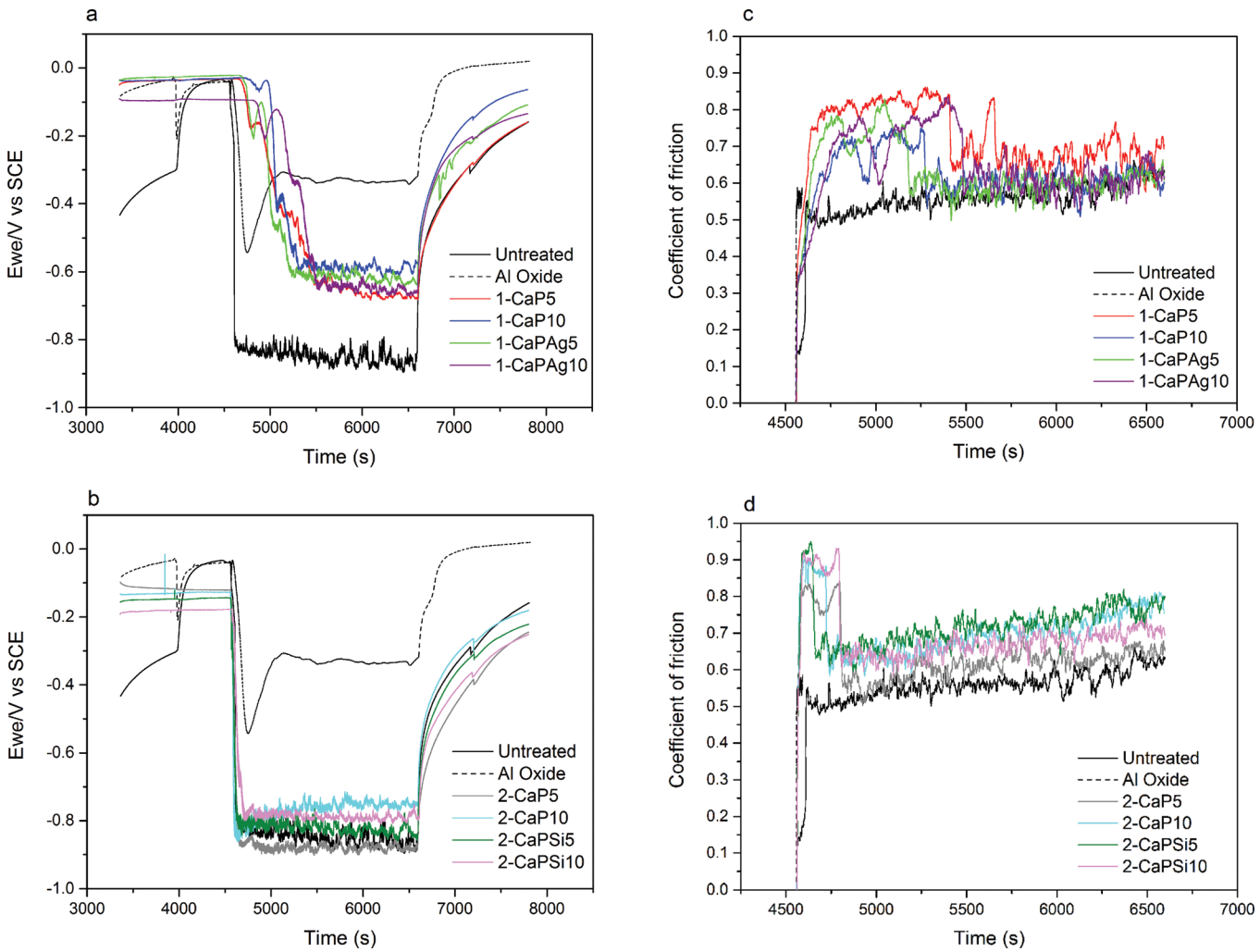

FIG. 5. Evolution of potential [(a) and (b)] and respective coefficients of friction [(c) and (d)] during tribocorrosion experiments for all the groups.

For the untreated samples, a sudden drop in potential was observed immediately after the sliding started. The potential value reached approximately −0.8 V, which remained stable until the end of the movement. This particular situation indicates that the natural passive film was disrupted or removed from the surface, and the Ti substrate was exposed to the electrolyte.[8,28]

Regarding the MAO-treated samples, two different behaviors were observed. The lower Ca concentration (2-MAO) presented similar drops (−0.8 V) and trend compared to the untreated group, in which the drop occurred immediately after the sliding started. On the other hand, when sliding started for 1-MAO with higher Ca concentration, the OCP did not change and remained unaltered for quite some time. The stable potential shows that the coating could withstand tribocorrosion exposure. Hence, the period until the coating exhibited stable potential can be called the coating lifetime. It is interesting to note that each coating shows different values, for example, approximately 5 min for 1-CaP5 and 1-CaPAg5 and 7 min for 1-CaP10 and 1-CaPAg10. The behavior obtained indicates that the MAO films produced with a larger amount of Ca and rutile in their microstructure were able to protect the Ti substrates from the damage posed by tribocorrosion events during a longer period of sliding.[28,29] After this period, the OCP values gradually decreased until they reached approximately −0.6 V, which can be associated with the presence of wear within the intermediate coating layers without reaching specifically the substrate. Also, the wear debris that accumulated at the contact zone may play a role in the overall potential drop and wear mechanisms. Previous studies have indicated that wear mechanisms might change from two-body (ball-coating) to three-body interactions due to the release of the wear debris (also clear from the SEM images).[26] The extension of the damage through the generated third bodies is further dependent on their geometry, size, hardness, and chemical properties.

For almost all groups, as soon as the sliding phase was over, the potential recovered to the initial stabilization period, indicating the repassivation of the Ti surface. However, the Al oxide group demonstrated more positive values after this time. This could mean that during the sliding period, the aluminum oxide particles used for the sandblasting procedure may have created a protective layer on the worn surface, which was subsequently produced during the tribocorrosion process.[41]

Although the Al oxide group presented a lower potential drop and smaller wear scar under free potential conditions, the same protective behavior was not observed under potentiodynamic mode. When a potential was applied during the sliding period, the depassivation was predominant on the repassivation event (Fig. 6). Such a variation in corrosion kinetics during the sliding potentially demonstrates the effectiveness of the coated samples. Furthermore, it was proven that infection, the presence of nicotine and soft drinks with varying *p*H levels might impose challenges on the implant surfaces by shifting the normal potential to very anodic values.[25,42,43] It can be noted that 1-CaP10 and 1-CaPAg10 had their potentiodynamic curves shifted to the upper-left region of the graph, demonstrating nobler potential and lower current compared to other groups.

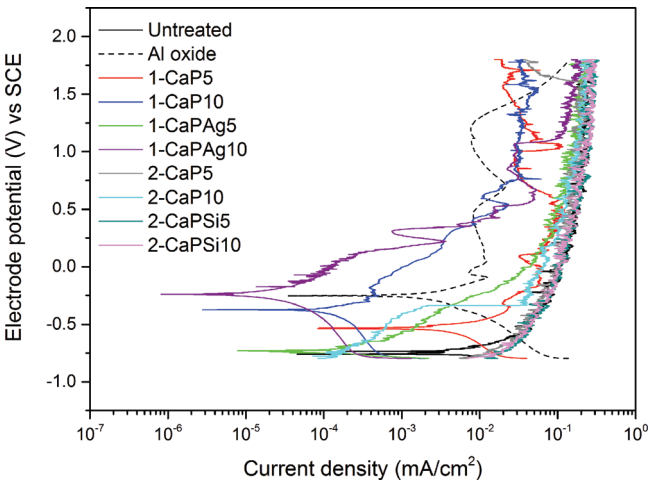

FIG. 6. Potentiodynamic curves with sliding time for all the studied groups. Note the shift of the curves to the upper-left area of the graph for 1-CaP10 and 1-CaPAg10 groups.

In WLI, 3D images of the wear scars obtained after the tribocorrosion experiments can be observed in Fig. 7. Regarding the resultant wear scars, it can be noted that Al oxide presented a narrow and shallow wear track, followed by the 1-MAO samples treated for 10 and 5 min. The untreated and 2-MAO groups (lower Ca concentration) had the widest and deepest wear scars. These results can be explained by the higher microhardness values obtained for the Al oxide samples, which lead to lower wear rates.

The relevant SEM images of the wear scars obtained after tribocorrosion testing for the MAO-treated and control groups are shown in Fig. 8. Four different patterns were determined (viz., untreated, Al oxide, 1-MAO, and 2-MAO). The untreated group presented the worst scenario with a larger wear scar; the Al oxide samples presented the narrowest wear track. Within the MAO-treated samples, 1-MAO was able to provide a more protective barrier compared to 2-MAO. The worn surfaces display the appearance of multiple striations, suggesting evidence of a predominant abrasive behavior.[44] The wear track is characterized by striations following the direction of the movement with the presence of material detachment at the sliding area. The untreated groups showed the presence of well-defined grooves and widened cracks, whereas the MAO-treated groups exposed less area of surface damage, suggesting a better performance dictated by the biomimetic barrier. The interface between the film and the wear track can also be observed. Differences in film thickness of the 1-MAO and 2-MAO groups are evident. This re-emphasizes the better tribocorrosion performance of higher Ca concentration groups (1-MAO).

Regarding the coefficient of friction [Figs. 5(c) and 5(d)], the values obtained for MAO-treated samples were slightly higher than those recorded for the control groups (≈0.55) at the beginning of the sliding period. The differences can be attributed to the surface characteristics (e.g., topography and

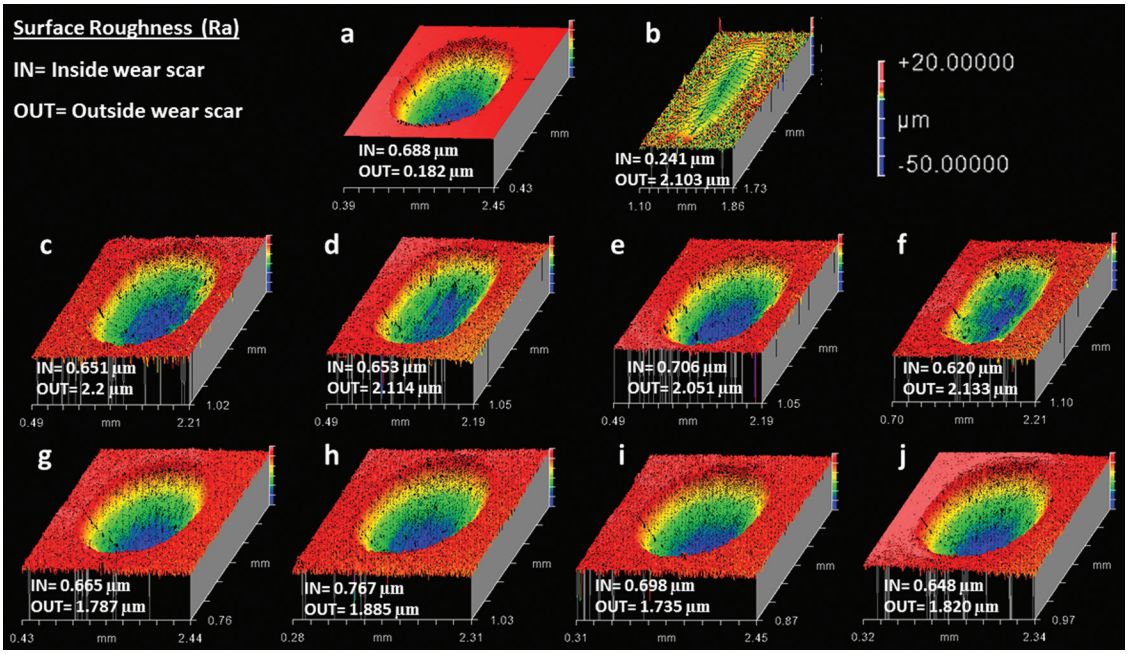

FIG. 7. White light interferometry of the wear scars after tribocorrosion experiments: (a)–(j) Untreated, Al oxide, 1-CaP5, 1-CaP10, 1-CaPAg5, 1-CaPAg10, 2-CaP5, 2-CaP10, 2-CaPSi5, and 2-CaPSi10, respectively.

crystalline structure) of anodized versus nonanodized samples. After the initial period of sliding, a smoother surface was obtained, and similar COF values were reached with no significant differences between them. These results are consistent with those reported elsewhere.[28] The increase in friction data presented upon the sliding process corresponds to the initial removal of the crushed and smeared surface layers from the coupled contacting surfaces.[8] The released fragments or wear debris during mechanical motion explain the severity of the tribological stresses and high frictional forces during the tribocorrosion process.[44] Such a severe process may generate more wear particles and participate in the wear process, resulting in the three-body process.[8] Furthermore, plastic deformation of the Ti surface along the wear track takes place due to the interaction of the Ti surface with a harder ceramic counter material (alumina) at a high Hertzian contact pressure (800 MPa). Hence, it is clear that the tribocorrosion process involved several wear mechanisms, such two-bodies, three-bodies, abrasion, and grooving. However, it is worth mentioning that delamination of the coating is not observed, as was expected from the other coatings. In fact, delamination of the coating is the main limiting factor behind the lack of use for biomedical applications. Further studies are required to explore the specific wear mechanisms and synergistic interaction of the wear and corrosion in the tribocorrosion process.

The average surface roughness (Ra) was analyzed in each of the specimens, as shown in Fig. 7. The values were taken from inside and outside the wear scar using WLI. The untreated group displayed a rougher surface inside the wear track compared to their outside boundaries. On the other hand, the opposite trend was obtained for the treated groups, in which a smoother area was attained on the worn surfaces. This situation is expected due to the porous and irregular surface morphology obtained after performing the corresponding treatments.

C. Cell culture characterization

As the result of the tribocorrosion experiments, two control groups (viz., untreated and Al oxide) and two experimental groups (1-CaP10 and 1-CaPAg10), which showed superior tribocorrosive behavior, were selected for further biological tests.

1. SEM analysis

The early stage of cell material interactions is characterized by the initial adhesion and spreading activities of the cells, which may influence the cells' proliferation and differentiation.[45]

At the early attachment time [Figs. 9(a)–9(d)], the hMSCs cultured onto the treated surfaces (Al oxide, 1-CaP10, and 1-CaPAg10) presented more of a spreading cell morphology compared to the untreated surfaces. After four days [Figs. 9(e)–9(h)], the cells were all well spread on the surface, although fewer cell projections were observed on the polished surface. At higher magnification, well-defined cells with longer pseudopodia connections extending over the treated surfaces were noticed, suggesting firm cell anchorage to the surfaces. The porous projection of the MAO-treated samples seems to guide the cells' morphology and attachment.[47,48] It is noticeable that the surface structure and chemistry may influence the cell attachment, spreading, and morphology, suggesting a more favorable cell response on MAO-treated surfaces.[49]

2. Fluorescence analysis

In general, the images show cells with cytoplasmic extensions (stained in red) with a central spherical nucleus

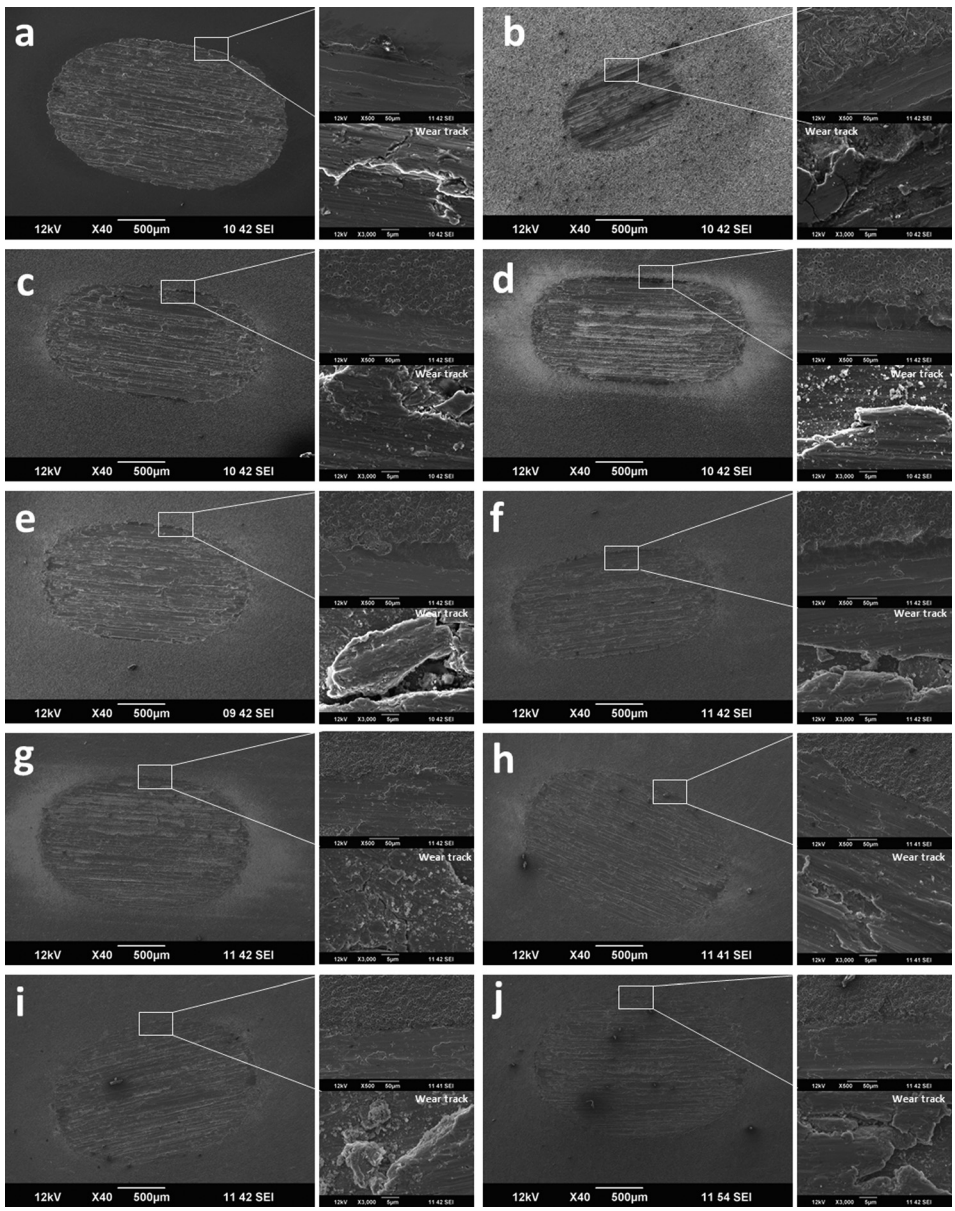

FIG. 8. SEM micrographs of the wear tracks on control and MAO-treated samples after the tribocorrosion tests (8.5 N, 3 mm, 1 Hz, 2000 cycles). (a) Untreated, (b) Al oxide, (c) 1-CaP5, (d) 1-CaP10, (e) 1-CaPAg5, (f) 1-CaPAg10; (g) 2-CaP5, (h) 2-CaP10; (i) 2-CaPSi5, and (j) 2-CaPSi10. The interface images are shown in the upper-right corner and the wear track in the lower corner of each corresponding group.

(stained in blue). The cells exhibited a well-organized and well-defined actin cytoskeleton, reflecting normal behavior.

In 3-h culture, cells on treated groups (Al oxide and MAO-treated groups) demonstrated more stretched shapes, containing more filopodia formation, than those in the untreated group (Fig. 10). The elongated and widely spread appearance corroborates the SEM results. From days 1 to 6 of cell culture, the number of cells on the different surfaces gradually increased, indicating that the sample surfaces are conducive to cell proliferation.[10]

3. MTT assay

An MTT assay was performed to investigate the viability of cells cultured on the modified Ti surfaces. The MTT mechanism is based on the mitochondrial succinate dehydrogenase within viable cells, forming blue formazan crystals.[46] Figure 11 shows the absorbance of formazan produced by hMSCs adhering to different Ti surfaces after culture for 1, 3, and 6 days. All surfaces tended to present higher cell viability over time. In this way, the number of viable cells significantly increased from day 1 to day 6 ($p < 0.05$). Although 1-CaP10 group had a lower cell viability on day 1 ($p < 0.05$), on the other days (3 and 6), all surfaces had similar values of cell viability. These results are in accordance with those presented elsewhere.[46,50–53] This indicates that cell viability may not only be influenced by surface characteristics, such as roughness, topography, or chemical composition. Other factors could also be involved. Therefore, osteogenic cell differentiation is relevant to be addressed.

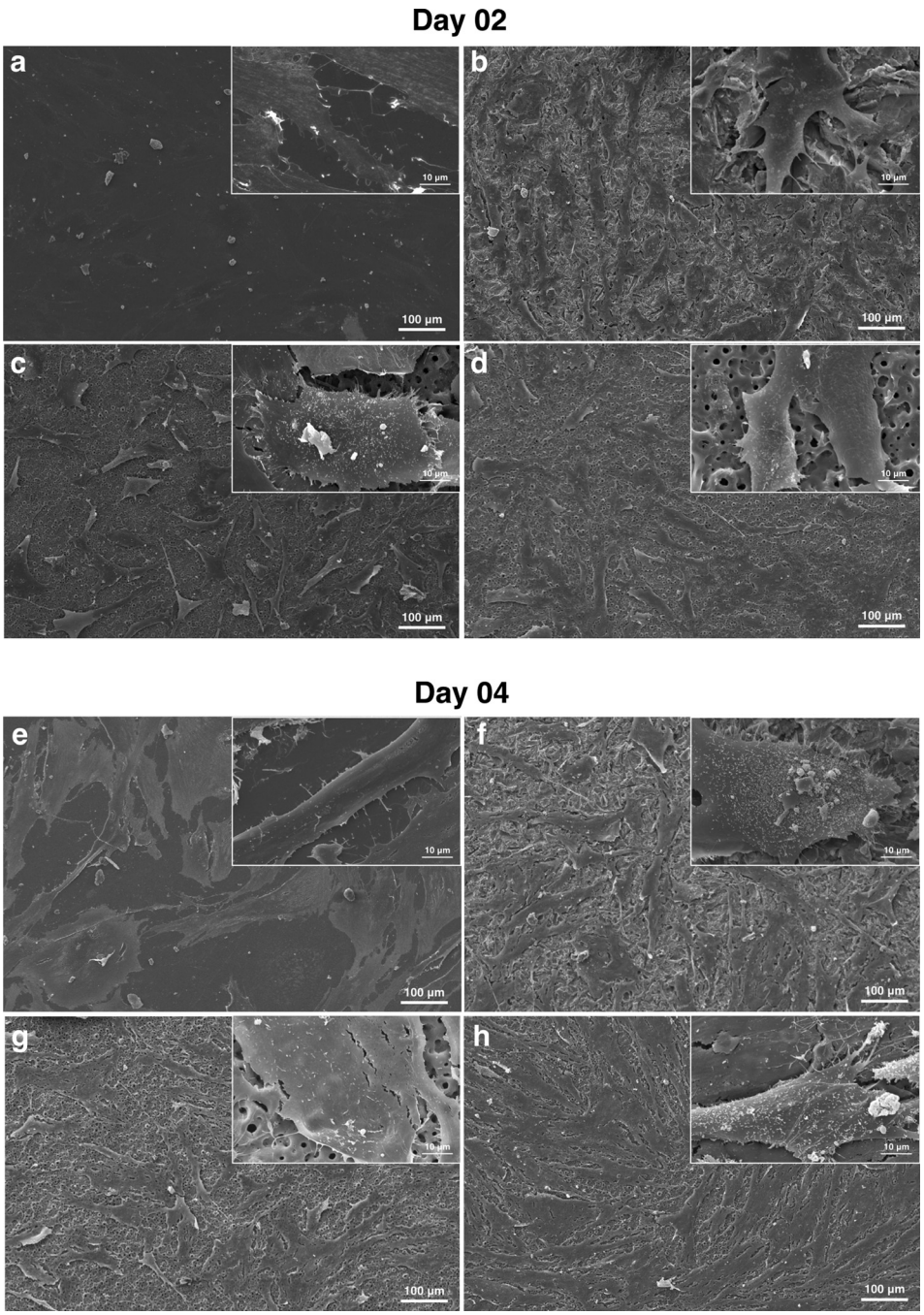

FIG. 9. Cellular morphology of hMSCs adhered to different Ti surfaces: untreated [(a) and (e)]; Al oxide [(b) and (f)]; 1-CaP10 [(c) and (g)]; and 1-CaPAg10 [(d) and (h)] at days 2 and 4. Higher magnification on the upper-right corner of each image (×2000).

4. Matrix formation analysis

Regarding the quantification of collagenous [Fig. 12(a)] and noncollagenous [Fig. 12(b)] proteins, the deposition presented a greater tendency to increase over time for the MAO-treated samples, highlighting the 1-CaPAg10 group for noncollagenous proteins ($p < 0.05$). Higher quantities of collagenous and noncollagenous proteins were observed on MAO-treated surfaces than for the untreated and Al oxide groups ($p < 0.05$) for both 10 and 17 days. No significant differences were found for the amount of deposited proteins between the untreated and Al oxide surfaces ($p > 0.05$).

According to Sabattini *et al.*,[53] a proteic layer is immediately formed over the material surface, either from the culture medium (*in vitro*) or from biological fluids (*in vivo*); this interface modulates the cascade of cellular behavior and response, such as adhesion, spreading, proliferation, and differentiation. Surface features such as topography and composition can affect the protein adsorption characteristics. Also, the mineralization process is influenced by matrix proteins, which can be collagenous or noncollagenous, so that a wide range of matrix proteins may have the potential to regulate cell activity.[54]

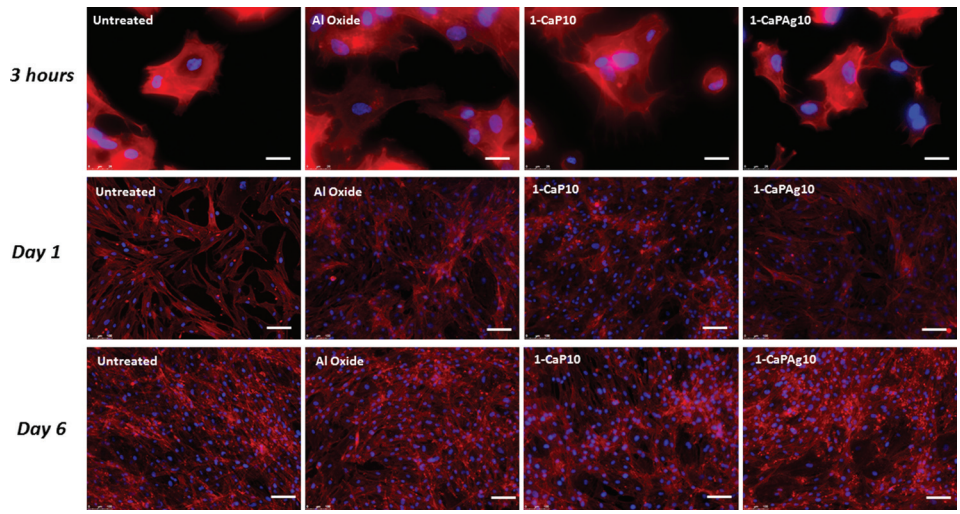

FIG. 10. Fluorescence images of hMSCs adhered to polished titanium (untreated), SLA surface (Al oxide) and MAO-treated samples. Cells were stained with actin filaments (red) and cell nuclei (blue). Scale bar: 25 μm (3 h) and 100 μm (days 1 and 6).

5. qRT-PCR analysis

A quantitative RT-PCR was performed to investigate the osteoblastic differentiation of hMSCs cultured on the different substrates tested. Bone-related genes were selected to evaluate the osteoblastic differentiation. RUNX2 is a fundamental transcription factor that regulates osteoblastic differentiation and is important during the stages of bone formation from differentiation of mesenchymal cells to osteoblast lineage.[55,56] Collagens are fibrillar proteins present in the extracellular matrix and give structural support to the cells, which may exert influence on the mineralization process.[54] TGFβ is the most abundant of all the known growth regulatory factors in bone. It may have a chemotactic function, which increases osteoblast migration to sites of resorption. Bone morphogenic proteins (BMP) are members of the TGFβ family that share the same ability of stimulating bone formation.[54] ALP activity is considered an early criterion to evaluate the differentiation level of the mineralization of osteoblasts, also a marker of the early stage of osteogenic differentiation.[47,53,57] OC is the most abundant noncollagenous protein in bone and is also used clinically as a marker of osteoblast activity.[54,57]

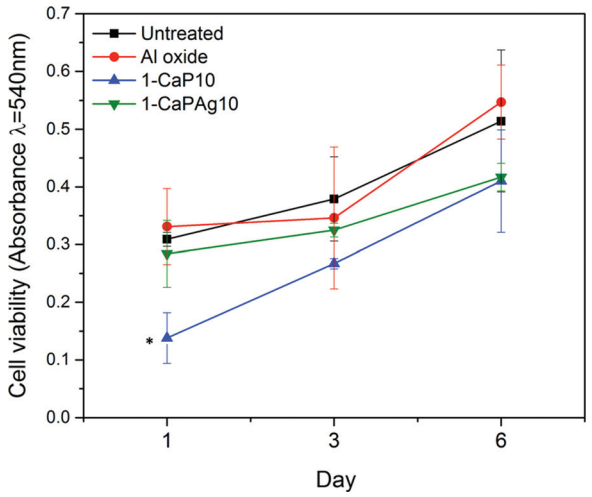

FIG. 11. MTT viability assay. Absorbance expressed as a measure of cell viability from hMSCs cultured onto smooth Ti surface (untreated), Al oxide, 1-CaP10, and 1-CaPAg10. *Significant difference compared to other groups ($p < .05$, Tukey HSD test).

Figure 13 shows the gene expression of ALP, BMP-2, OC, Col-1, RUNX2, and TGF-β1. In general, the gene expression was higher for the Ca and P groups (1-CaP10 and 1-CaPAg10) than for the untreated group. The osteogenic genes' expression was significantly enhanced by the addition of Ca and P in the surface, which suggests that the incorporation of some bioactive elements such as Ca and P can play a significant role in the calcification of bone matrix, bone growth, and osteoblastic differentiation.[10,15] The Ca and P contents and topography for both MAO-treated groups were quite similar, which demonstrates the similarity in PCR results. In particular, the Ag nanoparticles in the case of 1-CaPAg10 may have exerted some influence on the *in vitro* mineralization potential. Further investigation into the precise mechanism through which Ag nanoparticles affect osteogenic gene expression is required.

Bone matrix maturation is associated with the expression of ALP and several noncollagenous proteins. It is thought that these CaP-binding proteins help regulate ordered deposition of minerals by regulating the formation of hydroxyapatite crystals regarding quantity and size.[55]

It is interesting to note that in both matrix formation and qRT-PCR analyses, the cells presented higher collagen expression values when cultured on MAO-treated surfaces compared to control. Also, with undifferentiated hMSC, the CaP-enriched surfaces first decelerated cell proliferation and subsequently seemed to induce osteoblastic differentiation. Therefore, this interesting behavior may be related to the significantly higher degrees of anchorage observed for CaP groups compared to the smooth surface.[53]

In general, MAO-treated samples demonstrated good performance regarding tribocorrosion behavior, mechanical

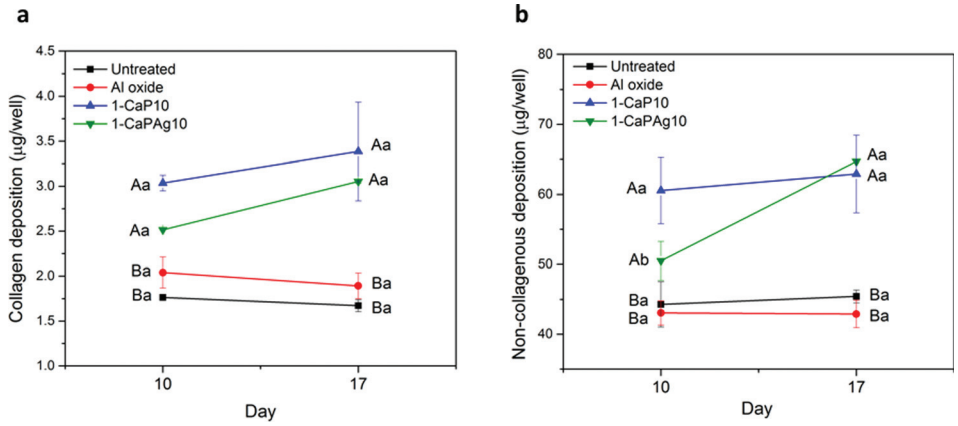

FIG. 12. (a) Collagen proteins and (b) noncollagenous quantification by Sirius red-based colorimetric assay at days 10 and 17. Different letters represent significant difference, uppercase letter for surface treatments and lowercase letter for times ($p < 0.05$; Tukey HSD test).

properties, and further enhancement of cell responses, which may result in better osseointegration. We have suggested the potential of using biomimetic coatings to improve titanium dental implant biocompatibility. However, as it is an *in vitro* study, there are some limitations. In the future, animal studies need to be performed to gain a better understanding of tribocorrosion and bone–implant interaction under daily activity simulations.

IV. CONCLUSIONS

Based on our results, the following conclusions can be drawn:

(1) Bioactive Ti-coatings doped with higher Ca concentrations were able to improve surface characteristics such as topography, chemical composition, the thickness of the coating, crystalline structure, and tribocorrosive behavior.
(2) Tribocorrosion studies have demonstrated the possible wear mechanisms and the role of wear debris in the degradation process. The high amount of Ca and microstructure of the coating play an important role in enhancing the tribocorrosion resistance of the coating.
(3) Ca and P additions resulted in a more favorable cellular response with higher osteogenic gene expression level and matrix formation, which may influence the calcification of bone matrix, in bone growth and osteoblastic differentiation.
(4) The incorporation of Ag nanoparticles in the oxide layer resulted in improved tribocorrosion resistance and cellular responses without causing any damage to hMSCs.

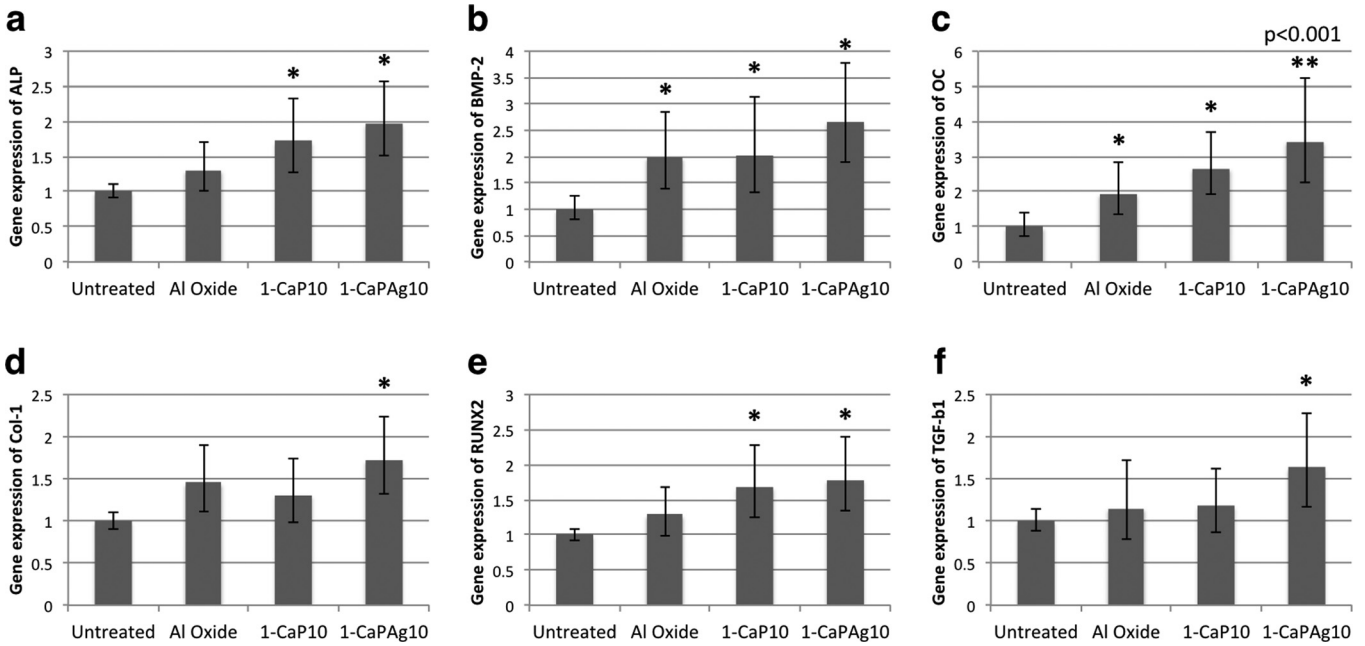

FIG. 13. Relative osteogenic gene expression obtained from qRT-PCR results. (a) ALP, (b) BMP-2, (c) OC, (d) Col-1, (e) RUNX2, and (f) TGF-b1. A significant difference was noted between the treated groups and the untreated group (*$p < 0.05$; **$p = 0.001$; Tukey HSD test).

ACKNOWLEDGMENTS

The authors would like to thank the University of Illinois at Chicago for providing the facilities to perform this study; Rush University Medical Center on behalf of R. Urban for the SEM facility; Denise Carleto Andia for providing the human bone marrow stromal cells for some cell experiments; Rafael Parra from Univ Estadual Paulista (Sorocaba, Brazil) for his contribution and support in the Plasma Technology Laboratory; the Coordination for the Improvement of Higher Level Personnel (CAPES) from Brazil for the doctoral fellowship of the first author (PDSE Proc. 11838-13-2); the State of Sao Paulo Research Foundation (FAPESP) for Grant No. 2013/08451-1; the National Science Foundation (NSF) for Grant No. 1067424; and finally financial support from NIH R03 AR064005.

[1]P. Malo, M. D. Araujo Nobre, A. Lopes, and R. Rodrigues, J. Prosthodontics **24**, 263 (2014).
[2]R. Doh, W. Park, K. Kim, and B. Jung, J. Prosthodontics **24**, 499 (2014).
[3]N. K. Kuromoto, R. A. Simão, and G. A. Soares, Mater. Charact. **58**, 114 (2007).
[4]L. Lara Rodriguez, P. A. Sundaram, E. Rosim-Fachini, A. M. Padovani, and N. Diffoot-Carlo, J. Biomed. Mater. Res., B **102**, 988 (2014).
[5]D. Siva Rama Krishna, Y. L. Brama, and Y. Sun, Tribol. Int. **40**, 329 (2007).
[6]M. Nakagawa, S. Matsuya, and K. Udoh, Dent. Mater. J. **21**, 83 (2002).
[7]F. Nikolopoulou, Implant Dent. **15**, 372 (2006).
[8]A. C. Vieira, A. R. Ribeiro, L. A. Rocha, and J. P. Celis, Wear **261**, 994 (2006).
[9]J. C. Souza, M. Henriques, R. Oliveira, W. Teughels, J. P. Celis, and L. A. Rocha, Biofouling **26**, 471 (2010).
[10]C. Della Valle, L. Visai, M. Santin, A. Cigada, G. Candiani, D. Pezzoli, C. R. Arciola, M. Imbriani, and R. Chiesa, Int. J. Artif. Organs **35**, 864 (2012).
[11]T. Akatsu, Y. Yamada, Y. Hoshikawa, T. Onoki, Y. Shinoda, and F. Wakai, Mater. Sci. Eng., C **33**, 4871 (2013).
[12]Y. T. Sul, Y. Jeong, C. Johansson, and T. Albrektsson, Clin. Oral Implants Res. **17**, 521 (2006).
[13]J. W. Park, Y. J. Kim, J. H. Jang, and H. Song, Clin. Oral Implants Res. **21**, 1278 (2010).
[14]Y. Vangolu, E. Arslan, Y. Totik, E. Demirci, and A. Alsaran, Surf. Coat. Technol. **205**, 1764 (2010).
[15]L. Franco Rde, R. Chiesa, M. M. Beloti, P. T. de Oliveira, and A. L. Rosa, J. Biomed. Mater. Res., A **88A**, 841 (2009).
[16]A. Zareidoost, M. Yousefpour, B. Ghaseme, and A. Amanzadeh, J. Mater. Sci. Mater. Med. **23**, 1479 (2012).
[17]H. P. Felgueiras *et al.*, J. Biomed. Mater. Res., B **103**, 661 (2014).
[18]F. C. Walsh, C. T. J. Low, R. J. K. Wood, K. T. Stevens, J. Archer, A. R. Poeton, and A. Ryder, Trans. IMF **87**, 122 (2009).
[19]C. A. Laurindo, R. D. Torres, S. A. Mali, J. L. Gilbert, and P. Soares, Mater. Sci. Eng., C **37**, 223 (2014).
[20]G. S. Shi, L. F. Ren, L. Z. Wang, H. S. Lin, S. B. Wang, and Y. Q. Tong, Oral Surg., Oral Med., Oral Pathol., Oral Radiol. **108**, 368 (2009).
[21]S. Li, J. Ni, X. Liu, X. Zhang, S. Yin, M. Rong, Z. Guo, and L. Zhou, J. Biomed. Mater. Res., B **100B**, 1587 (2012).
[22]L. P. Faverani, W. G. Assuncao, P. S. de Carvalho, J. C. Yuan, C. Sukotjo, M. T. Mathew, and V. A. Barao, PLoS One **9**, e93377 (2014).
[23]I. S. V. Marques, N. C. da Cruz, R. Landers, J. C. Yuan, M. F. Mesquita, C. Sukotjo, M. T. Mathew, and V. A. Barao, Biointerphases **10**, 041002 (2015).
[24]I. H. Liu, T. M. Lee, C. Y. Chang, and C. K. Liu, J. Dent. Res. **86**, 539 (2007).
[25]V. A. Barao, M. T. Mathew, W. G. Assuncao, J. C. Yuan, M. A. Wimmer, and C. Sukotjo, J. Dent. Res. **90**, 613 (2011).
[26]M. T. Mathew, S. Abbey, N. J. Hallab, D. J. Hall, C. Sukotjo, and M. A. Wimmer, J. Biomed. Mater. Res., B **100B**, 1662 (2012).
[27]P. Ponthiaux, F. Wenger, D. Drees, and J. P. Celis, Wear **256**, 459 (2004).
[28]S. A. Alves, R. Bayón, A. Igartua, V. Saénz de Viteri, and L. A. Rocha, Lubr. Sci. **26**, 500 (2014).
[29]A. C. Alves, F. Oliveira, F. Wender, P. Ponthiaux, J. P. Celis, and L. A. Rocha, J. Phys. D: Appl. Phys. **46**, 404001 (2013).
[30]Y. T. Sul, C. B. Johansson, Y. Jeong, and T. Albrektsson, Med. Eng. Phys. **23**, 329 (2001).
[31]H. Ishizawa and M. Ogino, J. Biomed. Mater. Res. **29**, 65 (1995).
[32]G. B. de Souza, G. G. de Lima, N. K. Kuromoto, P. Soares, C. M. Lepienski, C. E. Foerster, and A. Mikowski, J. Mech. Behav. Biomed. Mater. **4**, 796 (2011).
[33]A. M. G. Tavares, B. S. Fernandes, S. A. Souza, W. W. Batista, F. G. C. Cunha, R. Landers, and M. C. S. S. Macedo, J. Alloys Compd. **591**, 91 (2014).
[34]"NIST—National Institute of Stardards and Technology," 2010, http://srdata.nist.gov/xps/
[35]W. H. Song, Y. K. Jun, Y. Han, and S. H. Hong, Biomaterials **25**, 3341 (2004).
[36]Y. Han, S.-H. Hong, and K. Xu, Surf. Coat. Technol. **168**, 249 (2003).
[37]T. Beline *et al.*, Biointerphases **11**, 011013 (2016).
[38]I. S. V. Marques, V. A. R. Barão, N. C. da Cruz, J. C.-C. Yuan, M. F. Mesquita, A. P. Ricomini-Filho, C. Sukotjo, and M. T. Mathew, Corros. Sci. **100**, 133 (2015).
[39]I. S. V. Marques, M. F. Alfaro, N. C. da Cruz, M. F. Mesquita, C. Sukotjo, M. T. Mathew, and V. A. R. Barão, J. Mech. Behav. Biomed. Mater. **60**, 8 (2016).
[40]F. Contu, B. Elsener, and H. Böhni, Electrochim. Acta **50**, 33 (2004).
[41]D. Landolt, S. Mischler, M. Stemp, and S. Barril, Wear **256**, 517 (2004).
[42]D. Royhman, X. Dominguez-Benetton, J. C.-C. Yuan, T. Shokuhfar, C. Takoudis, M. T. Mathew, and C. Sukotjo, Clin. Implant Dent. Relat. Res. **17**, e352 (2015).
[43]I. Golvano, I. Garcia, A. Conde, W. Tato, and A. Aginagalde, J. Mech. Behav. Biomed. Mater. **49**, 186 (2015).
[44]M. J. Runa, M. T. Mathew, and L. A. Rocha, Tribol. Int. **68**, 85 (2013).
[45]Z. Zhang, B. Gu, W. Zhu, and L. Zhu, Exp. Ther. Med. **6**, 707 (2013).
[46]Y. Hu, K. Cai, Z. Luo, D. Xu, D. Xie, Y. Huang, W. Yang, and P. Liu, Acta Biomater. **8**, 439 (2012).
[47]A. Pae, S. S. Kim, H. S. Kim, and Y. H. Woo, Int. J. Oral Maxillofac Implants **26**, 475 (2011).
[48]K. R. Shin, Y. S. Kim, G. W. Kim, H. W. Yang, Y. G. Ko, and D. H. Shin, Appl. Surf. Sci. **347**, 574 (2015).
[49]S. A. Alves, R. Bayón, V. S. Viteri, M. P. Garcia, A. Igartua, M. H. Fernandes, and L. A. Rocha, J. Bio- and Tribo-Corros. **1**, 23 (2015).
[50]B. Feng, J. Weng, B. C. Yang, S. X. Qu, and X. D. Zhang, Biomaterials **25**, 3421 (2004).
[51]A. R. Ribeiro *et al.*, Mater. Sci. Eng., C **54**, 196 (2015).
[52]M. J. Runa, M. T. Mathew, M. H. Fernandes, and L. A. Rocha, Acta Biomater. **12**, 341 (2015).
[53]V. Bucci-Sabattini, C. Cassinelli, P. G. Coelho, A. Minnici, A. Trani, and D. M. Dohan Ehrenfest, Oral Surg., Oral Med., Oral Pathol., Oral Radiol. **109**, 217 (2010).
[54]A. Al-Qtaitat and S. Aldalaen, Am. J. Life Sci. **2**, 351 (2014).
[55]B. Clarke, Clin. J. Am. Soc. Nephrol. **3**, S131 (2008).
[56]D. P. Oliveira, A. Palmieri, F. Carinci, and C. Bolfarini, J. Biomed. Mater. Res. **102**, 1816 (2014).
[57]D. Kudelska-Mazur, M. Lewandowska-Szumiel, M. Mazur, and J. Komender, Cell Tissue Banking **6**, 55 (2005).